Contents

Model parameters

Parameter	Symbols used throughout	Default Value (Source or Derivation)	Units
Growth rate	μ	no default (optimized for through binary search process)	h^{-1}
Growth-associated maintenance requirement	GAM	35 (reduced from the amount in (Feist et al., 2007) to account for the portion directly modeled)	mmol ATP gDW^{-1}
Non-growth-associated maintenance requirement	NGAM	1 (reduced from the amount in (Feist et al., 2007) to account for the portion directly modeled)	mmol ATP gDW^{-1} h^{-1}
Unmodeled protein proportion of proteome	Q	0.45 (based on a rough approximation and (Scott et al., 2010))	unitless
proportion of RNA that is mRNA	f_{mRNA}	0.02 ((Bremer and Dennis, 1996) as 1-f_s and constant according to (Rosset et al., 1966))	unitless
proportion of RNA that is tRNA	f_{tRNA}	0.12 (Calculated using the formula 1-(1-f_s)-(1-f_t) with symbols taken from (Bremer and Dennis, 1996) and constant according to (Rosset et al., 1966))	unitless
proportion of RNA that is rRNA	f_{rRNA}	0.86 ((Bremer and Dennis,	unitless

		1996) as 1-f_t and constant according to (Rosset et al., 1966))	
Median enzyme efficiency		65 (In the range of the average enzyme from data in (Bar-Even et al., 2011))	s^{-1}
Flux ratio between the two NADH dehydrogenases		1:1 (NDH-1:NDH-2) (As in (Feist et al., 2007))	unitless
mRNA degradation constant	k_{deg}^{mRNA}	1/5 (≈80% of all mRNAs had half-lives between 3 and 8 min in (Bernstein et al., 2002))	min^1
Average molecular mass of RNA nucleotide	m_{nt}	324 (Bionumbers Database (Phillips and Milo, 2009) ID 104886)	Da
Average molecular mass of amino acid	m_{aa}	109 (Bionumbers Database (Phillips and Milo, 2009) ID 104877)	Da
Molecular mass of RNA component of ribosome	m_{rr}	1700 (Bionumbers Database (Phillips and Milo, 2009) ID 100119)	kDalton
Characteristic (average) molecular mass of a tRNA	m_{tRNA}	25000 (Bionumbers Database (Phillips and Milo, 2009) ID 101177)	Da
GC fraction for *E. coli* genomic DNA		0.507896997096 (Calculated from genome sequence given in (Blattner et al., 1997))	unitless
# ATP molecules hydrolyzed per nucleotide for RNA		0.25 (Assumed average as in (Thiele et al., 2009))	ATP molecules

degradation			
# nucleotides transcribed from DNA template before sigma factor dissociation		16 (Assumed average as in (Thiele et al., 2009))	nucleotides
# ATP molecules hydrolyzed per rho-dependent transcription termination event		3 (Assumed as in (Thiele et al., 2009))	ATP molecules

Growth rate-dependent demand reactions

DNA

base	# in genome given a total length of 4639675 with a GC fraction 0.5078	grams/mol (removed leaving group)	mol	grams
A	2283648.035	312.202	3.79209E-18	1.1839E-15
T	2283648.035	303.187	3.79209E-18	1.14971E-15
C	2356026.965	286.16	3.91227E-18	1.11954E-15
G	2356026.965	328.201	3.91227E-18	1.28401E-15
				Taking the sum, we find there are 4.73716E-15 grams of DNA per genome

The numbers used in the table above come from (Bremer and Dennis, 1996).

growth rate (doubling per hour)	genome equivalents	gDNA (given 4.73716E-15 grams of DNA per genome)	micrograms/ 10^9 cells	g_per_cell	% cell DNA
0	1*	4.73716E-15	80**	8E-14	5.921446222
0.6	1.6	7.57945E-15	148	1.48E-13	5.121250787
1	1.8	8.52688E-15	258	2.58E-13	3.30499324
1.5	2.3	1.08955E-14	433	4.33E-13	2.51627276
2	3	1.42115E-14	641	6.41E-13	2.217078149
2.5	3.8	1.80012E-14	865	8.65E-13	2.081063181

* This data point was assumed (not from (Bremer and Dennis, 1996)) given the fact that the number of genome equivalents in any given cell cannot be lower than 1.

** 80 fg per cell (and therefore 80 micrograms / 10^9 cells) comes from slowest growing cell in Figure 2b of (Burg et al., 2007). In this work, the mass of *Escherichia coli* was measured to be 110 +/- 30 fg in excess of the displaced buffer.

A sigmoid function was then fit to the '% cell DNA' column of the table above. The values from this function represent the final growth rate-dependent DNA demand requirements. The constraint was imposed as in genome-scale models of metabolism (Orth et al., 2011).

The final function is shown below:

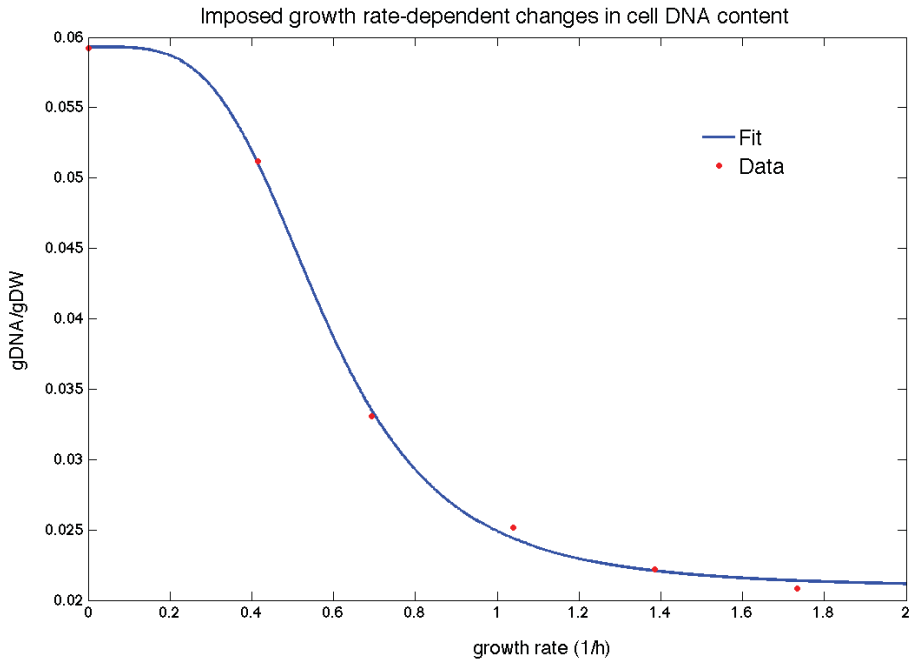

Cell wall

Biomass demand-like constraints were added to account for lipid/murein/LPS. These demands were formulated to be growth-rate-dependent, but the composition itself was assumed constant. The 'base shell composition' was constrained to be:

Component Abbreviation	Component Name	Molecular Weight	Demand Value
murein5px4p_Periplasm	two disacharide linked murein units, pentapeptide crosslinked tetrapeptide (A2pm->D-ala) (middle of chain)	1892.848 mg $mmol^{-1}$	0.01389 mmol gDW^{-1}
kdo2lipid4_Extra-organism	KDO(2)-lipid IV(A)	1840.033 mg $mmol^{-1}$	0.01945 mmol gDW^{-1}
pe160_Cytosol	phosphatidylethanolamine (dihexadecanoyl, n-C16:0)	691.972 mg $mmol^{-1}$	0.01786 mmol gDW^{-1}
pe160_Periplasm	phosphatidylethanolamine (dihexadecanoyl, n-C16:0)	691.972 mg $mmol^{-1}$	0.04594 mmol gDW^{-1}
pe161_Cytosol	phosphatidylethanolamine (dihexadec-9enoyl, n-C16:1)	687.94 mg $mmol^{-1}$	0.02105 mmol gDW^{-1}
pe161_Periplasm	phosphatidylethanolamine (dihexadec-9enoyl, n-C16:1)	687.94 mg $mmol^{-1}$	0.05415 mmol gDW^{-1}

To arrive at growth-rate-dependent cell wall dilution constraints, the cell surface area (SA) is calculated assuming that the cell is a cylinder with hemispherical caps:

Volume of the cell as a function of μ in μm^3, $v(\mu) = (l(\mu) - 2r(\mu)) * \pi * r(\mu)^2 + (4/3) * \pi r(\mu)^3$.
An empirical relation for $v(\mu)$ in μm^3 is $v(\mu) = 1.5 * 0.4 * 2^{\mu}$.
Given these 2 functions for volume, and also an empirical function for cell length as a function of μ in in μm, $l(\mu) = 1.5 * 2.6 * 2^{(ln(2)/3)\mu}$, one can obtain $r(\mu) = 1.5 * 0.15204137 * 2^{(ln(2)/3)\mu}$ through a least-squares optimization problem. A similar approach was taken in (Pramanik and Keasling, 1997), with the form of equations and numerical parameters taken from (Donachie and Robinson, 1987).

SA (in in μm^2) can then be calculated as function of μ using the equation:

$$SA(\mu) = 2 * \pi * r(\mu) * (l(\mu) - 2r(\mu)) + 4 * \pi * r(\mu)^2 .$$

Next we assumed as in (Pramanik and Keasling, 1997) that phosphatidylethanolamine makes up ~77% of the lipids, phosphatidylglycerol 18%, and cardiolipin 5%. We also assume an individual lipid has an area ~0.5 nm^2 and that 50% of the surface area is created by lipids (vs. proteins or other macromolecules). We also take into account that there are 4 individual lipid layers (2 lipid bilayers).

To calculate the grams of lipid per volume of cell as a function of growth rate, the following formula is used:

$$grams\ of\ lipid\ per\ volume(\mu) = \#\ lipid\ layers\ (4) * fraction\ of\ surface\ area\ lipids\ (0.5) * \ldots$$
$$SA(\mu) * 10^6 * (1/0.5\ nm^2) * (1/6.02 * 10^{23}) * wmw_{lipid}\ (g/mol)$$, where wmw_{lipid} is the weighted molecular weight (in g/mol) using the assumed composition and individual molecular weights of the lipids as follows: 734.03 g/mol for phosphatidylethanolamine, 827.11 g/mol for phosphatidylglycerol, and 1546 g/mol for cardiolipin. The 10^6 term is to correct the units, as SA(μ) is given in μm^2 (1 μm^2 = 10^6 nm^2).

Next, we convert this to lipid grams per gDW using an assumed cell density of 1.105 g / mL cell and an assumption that the dry weight of the cell is roughly 30% of its total weight.

Finally, we scale the demand reactions from the 'base shell composition' by a scalar that causes the bottom components listed in the table above to match this calculated growth-dependent demand for lipids.

Glycogen

The glycogen content of the cell was assumed constant in all simulations (independent of growth rate) performed in this study. It was set to 0.023 grams Glycogen per gDW of biomass based on the biomass objective function in (Feist et al., 2007).

The molecular weight for glycogen was taken to be 162.141 mg $mmol^{-1}$.

In silico growth media composition

Growth Nutrient (model identifier)	**Maximum Source Reaction Flux (mmol gDW^{-1} h^{-1})**
Chloride (cl)	1000
Magnesium (mg2)	1000

Molybdate (mobd)	1000
Nickel (ni2)	1000
Selenate (sel)	1000
Carbon Dioxide (co2)	1000
Calcium (ca2)	1000
Zinc (zn2)	1000
Phosphate (pi)	1000
Oxygen (o2)	1000
Manganese (mn2)	1000
Ammonium (nh4)	1000
Cob(I)alamin (cbl1)	1000
Sulfate (so4)	1000
Selenite (slnt)	1000
Copper (cu2)	1000
H+ (h)	1000
Potassium (k)	1000
D-Glucose (glc_DASH_D)	10
Cobalt (cobalt2)	1000
Water (h2o)	1000
Sodium (na1)	1000
Iron(II) (fe2)	1000
Iron(III) (fe3)	1000
Tungstate (tungs)	1000
Cesium (cs)	1000

All of these nutrients have the potential to be limiting for growth. An upper bound of 1000 mmol gDW^{-1} h^{-1} is used to simulate growth in batch culture whereas lower values are used in nutrient-limited simulations. The upper bound for D-Glucose uptake is set to 1000 for all

nutrient-limited simulations except when simulating D-Glucose limitation.

Non-default reaction bounds

As in iJO1366, the metabolic model for *Escherichia coli* (Orth et al., 2011), the following reactions are constrained by default to carry no flux to avoid unrealistic behaviors.

Reaction Name (abbreviation in iJO1366)	**Lower Bound**	**Upper Bound**
dihydropteridine reductase (DHPTDNR and DHPTDNRN in iJO1366)	0	0
succinate:aspartate antiporter (periplasm) (SUCASPtpp in iJO1366)	0	0
succinate:fumarate antiporter (periplasm) (SUCFUMtpp in iJO1366)	0	0
succinate:malate antiporter (periplasm) (SUCMALtpp in iJO1366)	0	0
succinate:D-tartrate antiporter (periplasm) (SUCTARTtpp in iJO1366)	0	0
catalase (CAT in iJO1366)	0	0
Formate-hydrogen lyase (FHL in iJO1366)	0	0
superoxide dismutase (SPODM and SPODMpp in iJO1366)	0	0

Optimization procedure

All ME-Model simulations presented in the manuscript maximize for growth rate subject to environmental substrate availability bounds. As the demand reactions and coupling constraints are functions of the organism's growth rate (μ), growth-rate optimization cannot be solved through linear programming as in metabolic models, which rely on a biomass objective function. Instead, to optimize for growth rate, we solve a sequence of linear programs (LPs) to search for the maximum growth rate, μ*, that still results in a feasible LP.

The proteome-limited (Janusian and Batch growth modes) simulations differ from strictly nutrient-limited (SNL) simulations due to different assumptions on enzyme saturation. Metabolic enzymes are assumed to be operating at their maximal capacity ($k_{eff} = k_{cat}$) in proteome-limited growth conditions, and operating below their maximal capacity ($k_{eff} < k_{cat}$) in SNL simulations.

By definition, the total biomass produced must be equal to the growth rate; proteome-limited (Janusian and Batch growth modes) simulations also differ from strictly nutrient-limited (SNL) simulations in how this constraint is enforced. In metabolic models, this constraint is imposed by the definition of the biomass objective function: the total mass in the biomass objective function sums to 1 g/gDW, and the flux through the biomass reaction is equal to the growth rate (h^{-1}). However, in the ME-Model, biomass production is split up into many dilution reactions for individual peptides, RNAs, and enzymes (to allow for variable biomass composition through gene expression) in addition to the DNA, Cell Wall, and Glycogen demand functions. Due to their different assumptions on enzyme saturation, the proteome-limited (Janusian and Batch growth modes) and SNL simulations differ in how the biomass production constraint is enforced, as explained below.

Batch and Janusian simulation procedure:
For simulations in the Batch and Janusian regions (when enzymes are assumed to be saturated), a ‘biomass capacity constraint’ is directly enforced. This additional row appended to the constraint matrix enforces that the sum of the masses of all biomass production reactions (component dilution and demand function fluxes) equals the growth rate.

After this additional constraint is added, the optimization problem is to maximize growth rate. As growth rate is an input to the matrix, we perform a binary search to find maximum feasible growth rate (and associated flux state). In searching for the maximum feasible growth rate, a series of linear programs (LPs) are solved to determine which are feasible. There is a unique maximum growth rate below which all LPs are feasible and above which all LPs are infeasible; therefore, in each step of the growth rate search, the objective of the LP will not affect the final maximum growth rate (see Figure below); in fact, the maximum feasible growth rate can be found without specifying a particular objective.

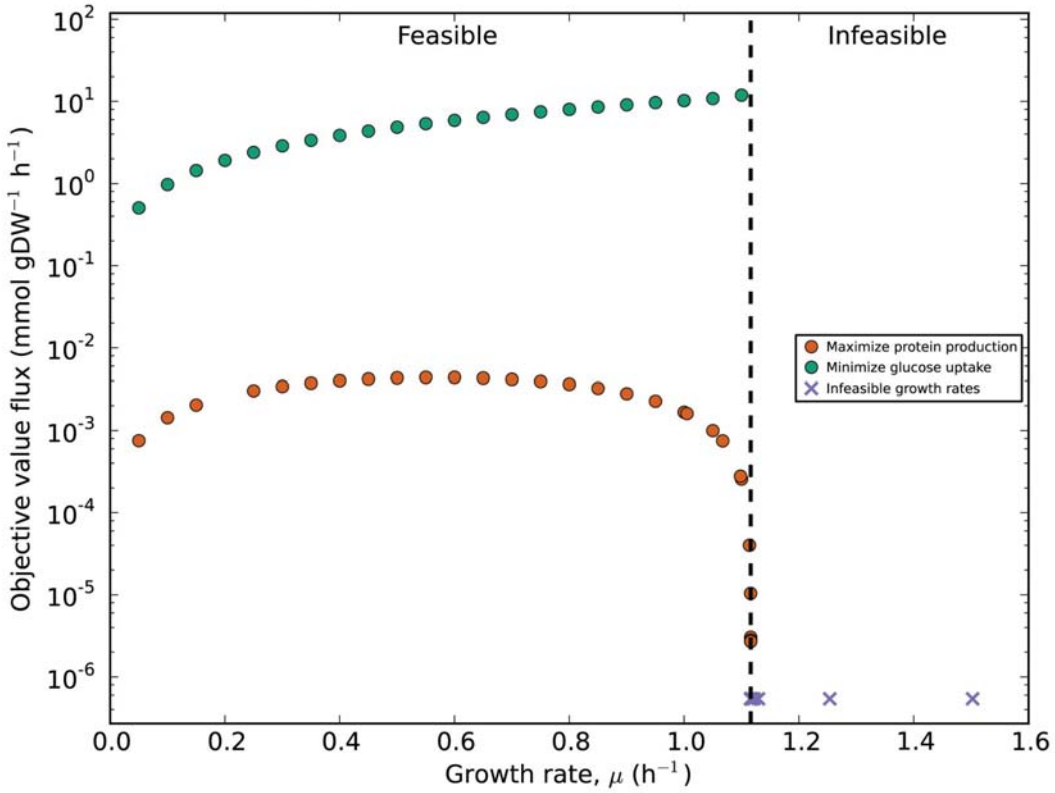

Depiction of proteome-limited optimization procedure. The black dashed line indicates the maximum feasible growth rate. Purple x's indicate growth rates that result in infeasible LPs (regardless of the objective). Green and orange circles indicate objective value fluxes at different growth rates with an objective of minimizing glucose uptake and maximizing the production of an unmodeled peptide (that does not catalyze any reaction in the model), respectively.

Strictly Nutrient-Limited simulation procedure:

For simulations in the Strictly Nutrient-Limited (SNL) region, a simple 'biomass capacity constraint' is insufficient. Under nutrient-limitation, if enzymes are assumed to be saturated, little protein is actually required to meet the requirements for growth. For this reason, simply adding a biomass capacity constraint and maximizing for growth rate (as in proteome-limited simulations, explained above), will result in little protein production and unnecessary RNA production simply to satisfy the biomass capacity requirement (as it is cheaper metabolically than protein), which is not accurate. So, to simulate nutrient-limited growth, we assume that the cell makes as much protein as possible (as it is generally the functional machinery of a cell); we then assume that this protein is all metabolic protein and the proteins are not saturated (so do not operate at k_{cat}). This is accomplished through two binary search procedures. In the first, the production of a 'dummy protein' is maximized, and a growth rate, μ*, is searched for where growth rate is equal to biomass dilution. The solution after this initial binary search will generally have a non-zero

dummy protein production. Then, the growth rate, μ*, is fixed and a binary search for the minimal fractional enzyme saturation (k_{eff} / k_{cat}) is found. At minimal fractional enzyme saturation and μ*, the dummy protein production will be 0. The qualitative shape of k_{eff} / k_{cat} vs. μ obtained matches empirical trends for individual enzymes and small-scale kinetic models (Figures 2E-2F, Supplementary Figure 1), supporting the validity of the simulation procedure. We recognize, however, that this is only an approximation as the scaling of metabolite levels will be specific to the nature of the nutrient limitation and that other proteins not directly used for growth are upregulated at lower growth rates.

Computational definition and identification of growth regions:
For most simulations (unless all uptakes of essential nutrients are unbounded, in which case it is a Batch simulation by definition), it is not known if the specific uptake bounds will result in a solution that lies in the Strictly Nutrient-Limited, Janusian, or Batch growth region. For these cases, they are first solved as SNL (see Strictly Nutrient-Limited simulation procedure). If no feasible solution is found where growth rate is equal to biomass dilution, the biomass capacity constraint is added and the problem is solved using the Batch and Janusian simulation procedure (see Batch and Janusian simulation procedure). Batch and Janusian regions are distinguished by comparing the optimal substrate uptake rate with the uptake bound imposed for essential nutrients. The growth region is defined as Janusian if the substrate uptake rate of any essential nutrient is equal to the imposed uptake bound; the growth region is defined as Batch if the uptake of all essential nutrients is lower than the imposed uptake bound (i.e., all essential nutrients are in excess).

With ME-Models, linear optimization begins to encounter scaling and/or infeasibility issues. To mitigate this problem, we used the SoPlex LP solver (freely available at http://soplex.zib.de) (Roland, 1996), which provides for solving the individual LPs using extended precision floating point numbers (80 bits) on x86 processors.

Discussion of central carbon flux predictions

Overall, the ME-Model flux predictions are more constrained than the M-model predictions (due to the associated gene expression constraints, Supplementary Table 7). At the two higher growth rates, the M-Model predictions for the flux through fructose-bisphosphate aldolase (fba), phosphotransacetylase (pta), succinate dehydrogenase (succ), and transaldolase (tal) are non-unique; in the ME-Model these fluxes are much more constrained (though at the lowest growth rate of 0.015 h^{-1}, the ME-Model has more slack due to numerical difficulties at the low growth rate). If a sequential optimization is performed in the M-Model where first biomass flux is maximized, then the sum of metabolic fluxes is minimized (subject to maintaining the optimal biomass production, an approach termed pFBA (Lewis et al., 2010)), the fluxes through central carbon metabolism become unique. The pFBA fluxes and ME-Model are very similar in the

nutrient-limited cases (Pearson r^2=0.99, r^2=0.98), but differ more in the Batch case (Pearson r^2=0.73). In the nutrient-limited cases, the ME-Model naturally accounts for the minimize-sum-of-fluxes sub-objective due to protein biosynthetic costs. In the case of Batch culture, there are important differences in the outliers of ME and pFBA predictions. In Batch culture, ME increases flux through pta, and decreases flux through succinate dehydrogenase (succ), malate dehydrogenase (mdh), isocitrate dehydrogenase (icd), citrate synthase (gltA), and fumarate (fum) (as occurs in the C13 data, Supplementary Figure 2B, but not in pFBA). Compared to fluxomic, the one main outlier in Batch culture for the ME-Model is pyruvate dehydrogenase (lpd); the ME-Model instead uses pyruvate formate lyase and the produced formate is then oxidized with formate dehydrogenase.

Computation of Gene Essentiality

In the ME-Model, gene knockouts are accomplished through deleting the translation reaction(s) for the peptide. Compared to the growth rates in the M-Model after single gene deletion, the ME-Model has many more genes that result in low but non-zero growth when knocked-out (Supplementary Table 4). We believe this is (at least partially) due to the multi-scale nature of the ME-Model, resulting in undetected numerical infeasibilities (i.e., the genes are actually essential, but required to be expressed below the precision of the linear programming solver at low growth rates). Based on the distribution of maximum growth rates after single gene deletions, we defined the growth rate cutoff for essential genes in the ME-Model to be 0.15 h^{-1} in glucose minimal media. We also computed the exact gene expression fluxes at 5% and 10% of the maximum growth rate in glucose minimal media (Supplementary Table 4) using exact simplex routines available in the QSopt_ex package (Applegate et al., 2007); some genes that are expressed very lowly in these solutions and are not called essential by the non-exact solver (Soplex) may actually be essential, but are not detectable without using a higher-tolerance solver. However, a gene that is called essential by the solver (Soplex) can be confidently labeled as essential in the model; so, the only potential difficulty is in genes that are essential in the model, but may not be called essential by the solver. These issues will be resolved with improved numerical methods.

Coupling constraints

(see next page)

Escherichia coli ME-Model Coupling Constraints

1. Variables and parameters used in derivations

To estimate the growth rate-dependent catalytic rates of enzymes we use the following variables and parameters.

P = total cellular protein mass (g gDW^{-1})
R = total cellular RNA mass (g gDW^{-1})
μ = specific growth rate (s^{-1})

f_{rRNA} = fraction of RNA that is rRNA
f_{mRNA} = fraction of RNA that is mRNA
f_{tRNA} = fraction of RNA that is tRNA

m_{aa} = molecular weight of average amino acid (g mmol^{-1})
m_{nt} = molecular weight of average mRNA nucleotide (g mmol^{-1})
m_{tRNA} = molecular weight of average tRNA (g mmol^{-1})
m_{rr} = mass of rRNA per ribosome (g)

k_{deg}^{mRNA} = first-order mRNA degradation constant (s^{-1})

Other than μ and P and R (which are functions of μ (eqation 1)), the others parameters are constants in derivations and their numerical values are listed in this document. To derive the catalytic rates of molecular machines, we rely on average values (e.g. average molecular weight of mRNA, protein). However, when transforming these into coupling constraints in the ME-Model, actual molecular weights of specific molecular species are used. For computations, all coupling parameters are computed to 4 significant digits for numerical purposes. In derivations, we use seconds as the time unit, though we convert these into hours for ME-Model computations.

2. Emperical RNA-to-Protein ratio

In (Scott et al., 2010) the RNA-to-Protein ratio was shown to increase linearly with growth rate, regardless of the specific environmental condition:

$$\frac{R}{P} = \frac{\mu}{\kappa_t} + r_o \tag{1}$$

For *E. coli* grown at 37 °C, (Scott et al., 2010) emperically found r_o=0.087 and κ_t=4.5 h^{-1}. We use these values in our derivations throughout.

3. 70S ribosomes

3.1. **Ribosomal translation rate and dilution.**

Assume all rRNA is incorporated into ribosomes.
Then: n_r = number of ribosomes = $\frac{Rf_{rRNA}}{m_{rr}}$

Assume proteins are stable and not degraded.
Then: P_s = Protein synthesis rate (aa/s) = $\frac{\mu P}{m_{aa}}$

3.2. **Hyperbolic ribosomal catalytic rate.**

Let:
k'_{ribo} = average translation rate of active ribosome (aa s^{-1})
f_r = fraction of ribosomes that are active
k_{ribo} = effective ribosomal translation rate (aa s^{-1})
$k_{ribo} = k'_{ribo}\ f_r$
$c_{ribosome} = \frac{m_{rr}}{m_{aa} f_{rRNA}}$

Then:
$k_{ribo} = \frac{P_s}{n_r} = \frac{c_{ribosome}\mu P}{R}$

Using (1),

$$k_{ribo} = \frac{c_{ribosome}\kappa_\tau \mu}{\mu + r_o \kappa_\tau} \tag{2}$$

Thus, translation rate is hyperbolic with respect to growth rate: $V_{max} = \kappa_\tau c_{ribosome}$ and $K_m = r_o \kappa_\tau$.

Using, parameters from , we get:
V_{max}=22.7 aa ribosome^{-1} s^{-1}
K_m=0.391 h^{-1}.

3.3. **Ribosomal coupling.**

Using equation (2), we derive an inequality constraint setting a lower bound on ribosomal dilution (to daughter cells)

The inequality is imposed in a manner that takes into account the length of each particular peptide that needs to be translated. Said another way, ribosomal machinery demands depend on the precise number of amino acids incorporated for each peptide in the model.

Let:
$V_{Ribosome\ Dilution}$ = dilution of ribosome (mmol ribosome $\mathrm{gDW}^{-1}\ \mathrm{s}^{-1}$)
$V_{Translation\ of\ peptide_i}$ = translation of $\mathrm{peptide}_i$ (mmol $\mathrm{peptide}_i$ $\mathrm{gDW}^{-1}\ \mathrm{s}^{-1}$)
$length(peptide_i)$ = number of amino acids in $\mathrm{peptide}_i$

Then:
$$V_{Ribosome\ Dilution} \geq \sum_i \left(\frac{length(peptide_i)}{k_{ribo}/\mu} * V_{Translation\ of\ peptide_i} \right)$$

4. RNA Polymerase

Let:
k_{rnap} = RNAP transcription rate (nucleotide $\mathrm{RNAP}^{-1}\ \mathrm{s}^{-1}$)

The transcription rate, k_{rnap}, is taken to be exactly 3 times the translation rate at all growth rates based on data from Table 1 from (Proshkin et al., 2010).

Then:
$k_{rnap} = 3k_{ribo}$

Using equation (2), we derive an inequality constraint setting a lower bound on ribosomal dilution (to daughter cells)

The inequality was imposed in a manner that takes into account the length of each particular transcription unit (TU) that needs to be transcibed. Said another way, RNA polymerase machinery demands depend on the precise number of nucleotides transcribed for each RNA in the model.

Let:
$V_{RNAP\ Dilution}$ = dilution of RNAP (mmol RNAP $\mathrm{gDW}^{-1}\ \mathrm{s}^{-1}$)
$V_{Transcription\ of\ TU_i}$ = transcription of TU_i (mmol TU_i $\mathrm{gDW}^{-1}\ \mathrm{s}^{-1}$)
$length(TU_i)$ = number of nucleotides in TU_i

Then:
$$V_{RNAP\ Dilution} \geq \sum_i \left(\frac{length(TU_i)}{k_{rnap}/\mu} * V_{Transcription\ of\ TU_i} \right)$$

5. mRNA coupling

5.1. **Dilution, degradation, translation reaction rates.**

For the derivation, assume that mass of mRNA transcribed, translated, degraded, and diluted is only in coding regions. In actuality, the molecular weight of mRNA will be higher due to untranslated regions, which is reflected in the values used in the ME-Model.

Let:
dil_{mRNA} = dilution of mRNA (mmol nucleotides gDW^{-1} s^{-1})
deg_{mRNA} = degradation of mRNA (mmol nucleotides gDW^{-1} s^{-1})
$trsl_{mRNA}$ = translation of protein from mRNA (mmol amino acids gDW^{-1} s^{-1})
$[mRNA]$ = mRNA concentration (mmol nucleotides gDW^{-1})

Then:
$dil_{mRNA} = \mu[mRNA]$
$deg_{mRNA} = k_{deg}^{mRNA}[mRNA]$
$trsl_{mRNA} = \frac{\mu P}{m_{aa}}$
$[mRNA] = \frac{Rf_{mRNA}}{m_{nt}}$

5.2. **Coupling.**

The mRNA dilution, degradation, and translation reactions are coupled in the ME-Model with linear inequalities as followed:

$dil_{mRNA} \geq \alpha_1 deg_{mRNA}$
$deg_{mRNA} \geq \alpha_2 trsl_{mRNA}$

The inequality formulation allows for some mRNA transcribed to not be translated, but it still must be diluted and degraded.

When the inequality constraints are operating at their bounds, α_1 and $alpha_2$ will then be:

$$\alpha_1 = \frac{dil_{mRNA}}{deg_{mRNA}} = \frac{\mu[mRNA]}{k_{deg}^{mRNA}[mRNA]} = \frac{\mu}{k_{deg}^{mRNA}}$$

$$\alpha_2 = \frac{3deg_{mRNA}}{trsl_{mRNA}} = \frac{3k_{deg}^{mRNA}[mRNA]m_{aa}}{\mu P} = \frac{3k_{deg}^{mRNA}Rf_{mRNA}m_{aa}}{\mu P m_{nt}}$$

Note: The factor of 3 above is to account for 3 nucleotides per amino acid.

5.3. **Hyperbolic mRNA catalytic rate.**

The above formulation also results in a hyperbolic mRNA catalytic rate.

Let:
k_{mRNA} = mRNA catalytic rate (mmol protein (mmol mRNA)$^{-1}$ hr^{-1})
$c_{mRNA} = \frac{m_{nt}}{f_{mRNA} m_{aa}}$.

Then:
$k_{mRNA} = \frac{trsl_{mRNA}}{[mRNA]} = \frac{c_{mRNA} \mu P}{R}$.

Using (1):
$k_{mRNA} = \frac{c_{mRNA} \kappa_\tau \mu}{\mu + r_o \kappa_\tau}$

Using parameters listed in this document, we get:
Vmax=$c_{mRNA}\kappa_\tau$ = 0.5 protein mRNA^{-1} s^{-1}
K_m = 0.391 h^{-1}.

6. tRNA coupling

6.1. **Rates of charging and dilution of tRNA.**

Let:
chg_{mRNA} = charging of tRNA (mmol tRNA gDW^{-1} s^{-1})
dil_{tRNA} = dilution of tRNA (mmol tRNA gDW^{-1} s^{-1})
$[tRNA]$ = tRNA concentration (mmol tRNA gDW^{-1})

Then:
$dil_{tRNA} = \mu [tRNA]$
$chg_{tRNA} = \frac{\mu P}{m_{aa}}$
$[tRNA] = \frac{R f_{tRNA}}{m_{tRNA}}$

6.2. **Coupling.**

The tRNA dilution and charging reactions are coupled in the ME-Model with linear inequalities as followed:

$dil_{tRNA} \geq \alpha chg_{tRNA}$

At the bound of equality,

$\alpha = \frac{dil_{tRNA}}{chg_{tRNA}} = \frac{R f_{tRNA} m_{aa}}{P m_{tRNA}}$

6.3. **Hyperbolic tRNA efficiency.**

The above formulation also results in a hyperbolic tRNA catalytic rate.

Let:
k_{tRNA} = tRNA catalytic rate (mmol protein (mmol tRNA)$^{-1}$ hr^{-1})
$c_{tRNA} = \frac{m_{tRNA}}{m_{aa} f_{tRNA}}$

Then:
$k_{tRNA} = \frac{chg_{tRNA}}{[tRNA]} = \frac{\mu P m_{tRNA}}{m_{aa} R f_{tRNA}} = \frac{c_{tRNA} \mu P}{R}$

Using (1):
$k_{tRNA} = \frac{c_{tRNA} \kappa_\tau \mu}{\mu + r_o \kappa_\tau}$

Using parameters in , we get:
Vmax=$c_{tRNA} \kappa_\tau$ = 2.39 aa tRNA^{-1} s^{-1}.
K_m = 0.391 h^{-1}.

7. Remaining Macromolecular Synthesis Machinery

For the remaining macromolecular synthesis machinery, we set $k_{cat} = 65\ (s^{-1})$ across all growth rates:

$$V_{Machinery_i\ Dilution} \geq \sum_i \left(\frac{1}{k_{cat}/\mu} * V_{Use\ of\ Machinery_i} \right)$$

8. Metabolic Enzymes

For metabolic enzymes, the catalytic rate is set to be proportional to the enzyme solvent accessible surface area (SASA).

Calculation of solvent accessible surface area (SASA):
$SASA Enzyme i = (Molecular Weight Enzyme i)^{\frac{3}{4}}$ based on the empirical fit from (Miller et al., 1987).

The specific enzyme efficiency value received for a given enzyme/complex was assumed to be linearly dependent on its SASA value. The mean of all the kinetic constants was centered at $k_{eff} = 65\ (s^{-1})$. Let $\underline{\underline{SASA}}$ denote a particular value after centering.

$$V_{Metabolic\ Enzyme_i\ Dilution} \geq \sum_i \left(\frac{1}{\underline{\underline{SASA}}_{Metabolic\ Enzyme_i}/\mu} * V_{Use\ of\ Metabolic\ Enzyme_i} \right)$$

This coupling is a gross approximation for an enzyme's kinetic information. Its purpose is to reward expression of large complexes (such as pyruvate dehydrogenase which is composed

of 12 AceE dimers, a 24-subunit AceF core, and 6 LpdA dimers), given these complexes have many more active sites (on average) than smaller enzymes. In the future, these values can be parameterized further using condition-specific multi-omics data.

Supplementary references

Applegate, D. L., Cook, W., Dash, S., and Espinoza, D. G. (2007). Exact solutions to linear programming problems. Operations Research Letters *35*, 693 - 699.

Bar-Even, A., Noor, E., Savir, Y., Liebermeister, W., Davidi, D., Tawfik, D. S., and Milo, R. (2011). The moderately efficient enzyme: evolutionary and physicochemical trends shaping enzyme parameters. Biochemistry *50*, 4402-4410.

Bernstein, J. A., Khodursky, A. B., Lin, P. H., Lin-Chao, S., and Cohen, S. N. (2002). Global analysis of mRNA decay and abundance in Escherichia coli at single-gene resolution using two-color fluorescent DNA microarrays. Proc Natl Acad Sci U S A *99*, 9697-9702.

Blattner, F. R., Plunkett, G., Bloch, C. A., Perna, N. T., Burland, V., Riley, M., Collado-Vides, J., Glasner, J. D., Rode, C. K., Mayhew, G. F., Gregor, J., Davis, N. W., Kirkpatrick, H. A., Goeden, M. A., Rose, D. J., Mau, B., and Shao, Y. (1997). The Complete Genome Sequence of Escherichia coli K-12. Science *277*, 1453-1462.

Burg, T. P., Godin, M., Knudsen, S. M., Shen, W., Carlson, G., Foster, J. S., Babcock, K., and Manalis, S. R. (2007). Weighing of biomolecules, single cells and single nanoparticles in fluid. Nature *446*, 1066-1069.

Donachie, W. D., and Robinson, A. C. (1987). Cell Division: Parameter Values and the Process. In Escherichia coli and Salmonella typhimurium. Cellular and molecular biology. Volumes I and II., Neidhardt, F. C., J. L. Ingraham, K. B. Low, B. Magasanik, M. Schaechter, and H. E. Umbarger, American Society for Microbiology), pp. 1578-1593.

Feist, A. M., Henry, C. S., Reed, J. L., Krummenacker, M., Joyce, A. R., Karp, P. D., Broadbelt, L. J., Hatzimanikatis, V., and Palsson, B. O. (2007). A genome-scale metabolic reconstruction for Escherichia coli K-12 MG1655 that accounts for 1260 ORFs and thermodynamic information. Mol Syst Biol *3*, 121.

Lewis, N. E., Hixson, K. K., Conrad, T. M., Lerman, J. A., Charusanti, P., Polpitiya, A. D., Adkins, J. N., Schramm, G., Purvine, S. O., Lopez-Ferrer, D., Weitz, K. K., Eils, R., Konig, R., Smith, R. D., and Palsson, B. O. (2010). Omic data from evolved E. coli are consistent with computed optimal growth from genome-scale models. Mol Syst Biol *6*, 390.

Miller, S., Lesk, A. M., Janin, J., and Chothia, C. (1987). The accessible surface area and stability

of oligomeric proteins. Nature *328*, 834-836.
Phillips, R., and Milo, R. (2009). A feeling for the numbers in biology. Proc Natl Acad Sci U S A *106*, 21465-21471.

Pramanik, J., and Keasling, J. D. (1997). Stoichiometric model of Escherichia coli metabolism: incorporation of growth-rate dependent biomass composition and mechanistic energy requirements. Biotechnol Bioeng *56*, 398-421.

Proshkin, S., Rahmouni, A. R., Mironov, A., and Nudler, E. (2010). Cooperation between translating ribosomes and RNA polymerase in transcription elongation. Science *328*, 504-508.

Roland, W. Paralleler und objektorientierter Simplex-Algorithmus. Technische Universität Berlin; 1996. p. Dissertation.

Rosset, R., Julien, J., and Monier, R. (1966). Ribonucleic acid composition of bacteria as a function of growth rate. J Mol Biol *18*, 308-320.

Figure S1. Metabolic enzyme activity under nutrient limitation.
A) Data on LacZ activity in *Klebsiella aerogenes* is used to calculate a value proportional to the fractional enzyme saturation at different growth rates in lactose minimal media. The o- (or p-) nitrophenol specific activity of LacZ (which is proportional to the lactose specific activity) is measured in lactose minimal media (Smith and Dean, 1972); the fractional enzyme saturation is then calculated assuming a constant biomass yield of 0.5 g Lactose / gDW.
B) The average effective catalytic rate (flux/enzyme) is reported for a small-scale kinetic model (Molenaar et al., 2009) at different growth rates under nutrient limitation.

Figure S2. Fluxomic fold changes.
A and B) Fold changes in ME-Model predicted and ^{13}C estimated metabolic fluxes are plotted. A) is the fold change between the fluxes shown in Figures 3A and 3B and B) is the fold change between fluxes shown in Figures 3B and 3C.

Figure S3. Growth rate-dependent gene expression under glucose-limitation.
ME-Model-computed fold changes (as a fraction of total proteome content) for all genes expressed in glucose minimal media from growth rates of 0.45 h^{-1} to 0.93 h^{-1} (chosen to span the Strictly Nutrient-Limited region) are plotted in rank order (grey points). Each colored diamond corresponds to the median fold change of all gene-enzyme pairs in a given cluster from Figure 4B. The error bar for each indicates the median absolute deviation (MAD) from the median fold change, provided this error is at least 2% of the median.

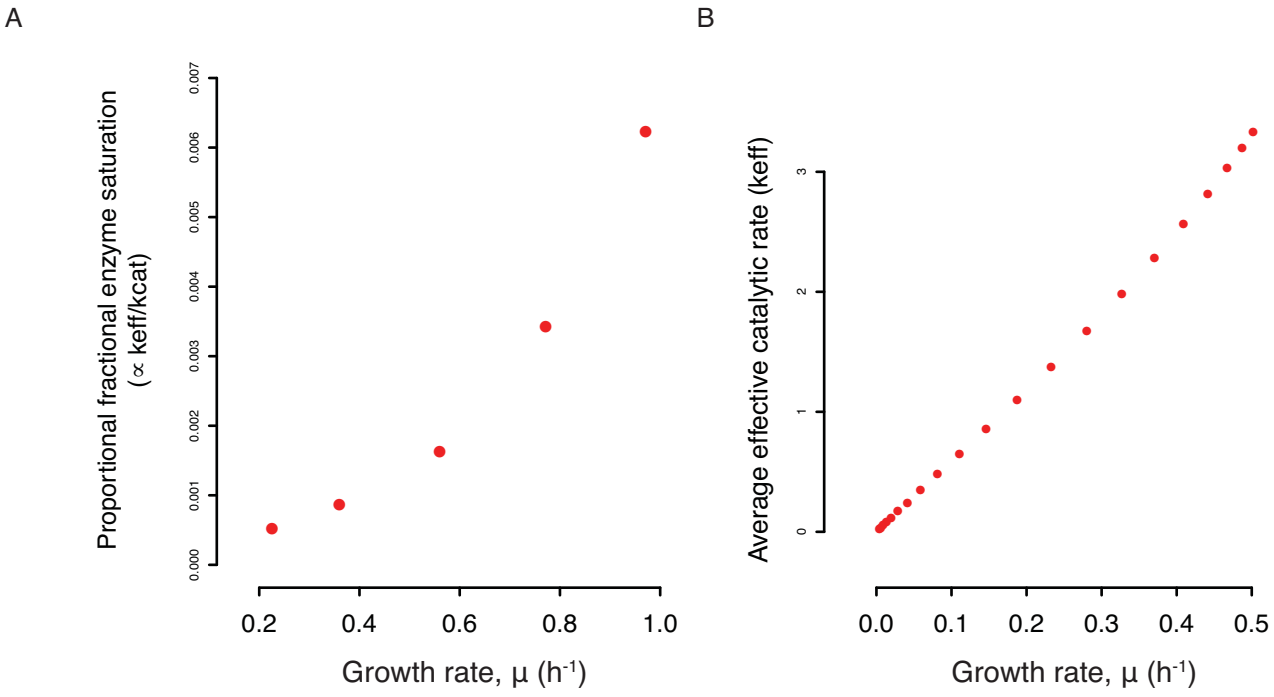
A
Proportional fractional enzyme saturation
(∝ keff/kcat)
0.000
0.001
0.002
0.003
0.004
0.005
0.006
0.007
0.2
0.4
0.6
0.8
1.0
Growth rate, μ (h-1)
B
Average effective catalytic rate (keff)
0
1
2
3
0.0
0.1
0.2
0.3
0.4
0.5
Growth rate, μ (h-1)

Figure S1

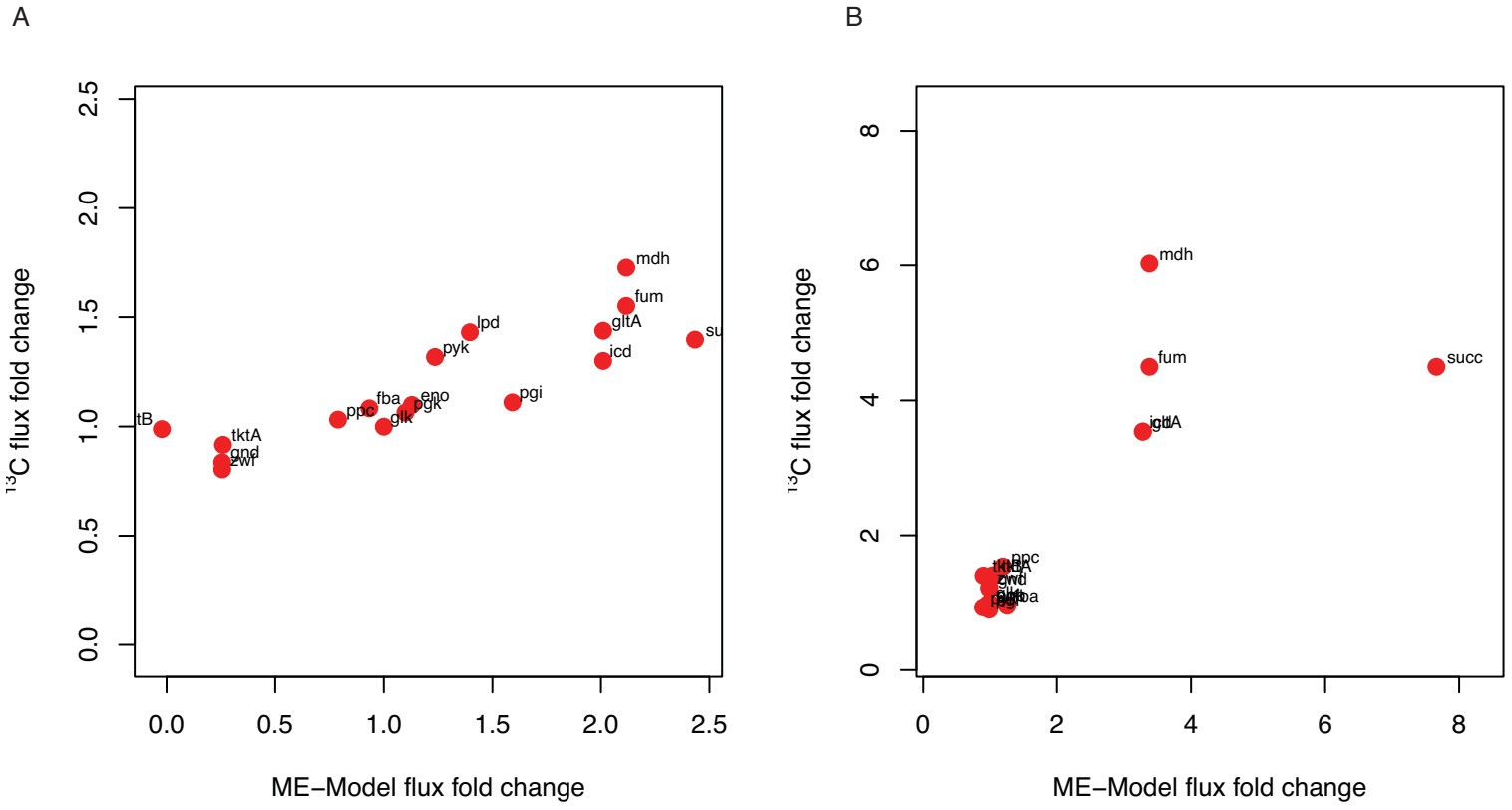
A
B
^{13}C flux fold change
ME−Model flux fold change
mdh
fum
gltA
icd
lpd
pyk
pgi
fba
eno
pgk
ppc
gnd
zwf
tktA
tB
su
succ
0.0
0.5
1.0
1.5
2.0
2.5
0
2
4
6
8

Figure S2

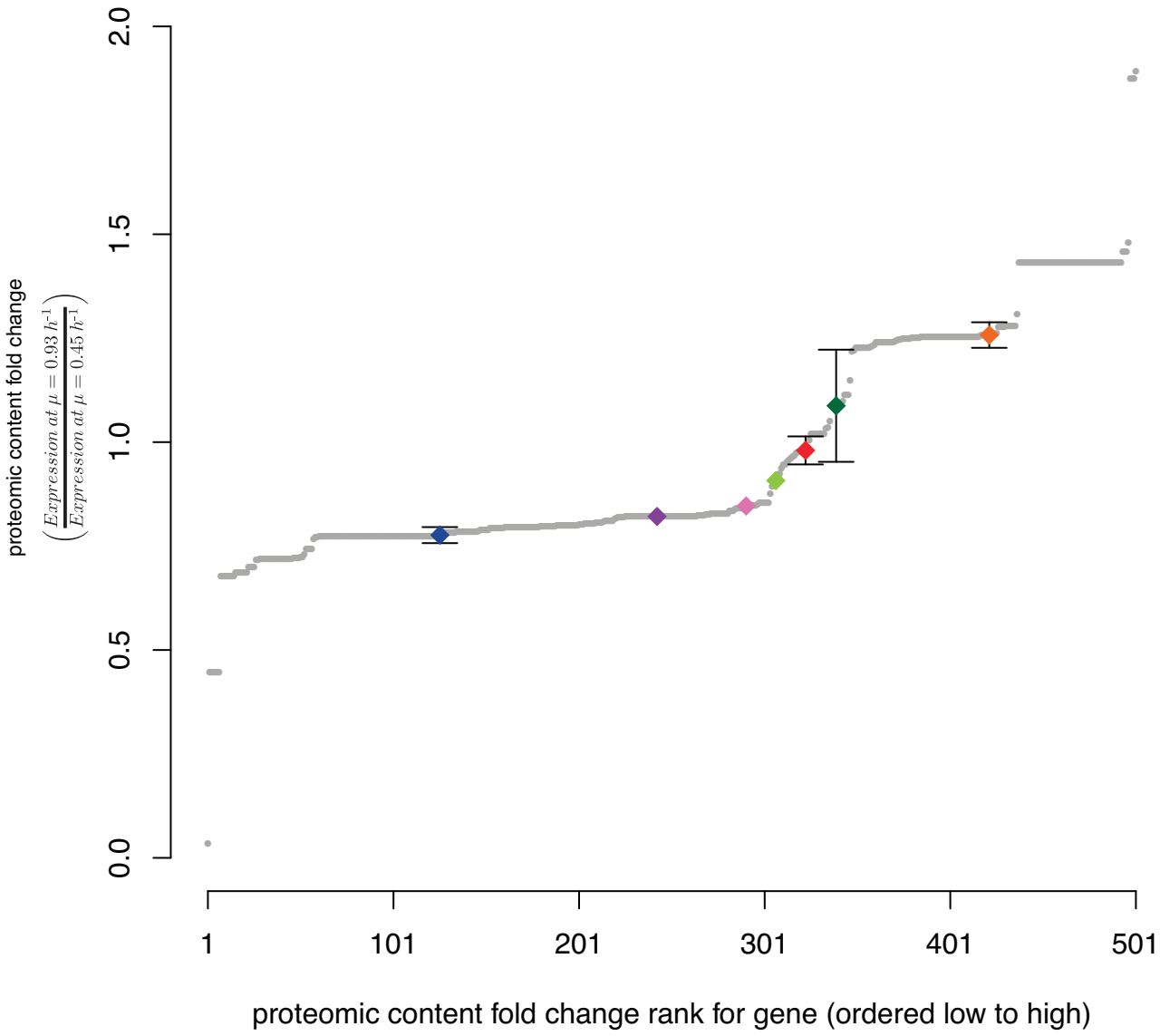
proteomic content fold change
$\left(\frac{Expression\ at\ \mu = 0.93\ h^{-1}}{Expression\ at\ \mu = 0.45\ h^{-1}}\right)$
0.0
0.5
1.0
1.5
2.0
1
101
201
301
401
501
proteomic content fold change rank for gene (ordered low to high)

Figure S3